

# Face Recognition Using the Diagonal Relative Gradient Method in a Low Illumination Environment

Deng-Yuan Huang<sup>1</sup>, Chun-Jih Lin<sup>1</sup>, Shr-Huan Dai<sup>1</sup>

<sup>1</sup>Department of Electrical Engineering, Dayeh University, Taiwan  
168, University Rd., Dacun, Changhua 51519, Taiwan  
kevin@mail.dyu.edu.tw; genzi.ltd@msa.hinet.net; plonker1989@gmail.com

Received January, 2014; revised March, 2014

---

**ABSTRACT.** *Face recognition has been widely applied in entry access control, criminal identification, financial withdrawal safety verification, and user identification in online transactions. However, illumination variation has persistently been a challenging problem in the domain of face recognition. Therefore, this study proposed an illumination variation processing method that can effectively resolve the low face recognition efficacy resulting from illumination variations. In this study, we developed the diagonal relative gradient (RG) method (hereafter referred to as the DRG method) to reduce the influence that variations in illumination have on face recognition. Rank transform was employed to further enhance human facial features. Subsequently, the dual-tree complex wavelet transform was used to extract the image features of human faces. Experimental results demonstrated that compared with traditional RG methods, the proposed DRG method was superior in extracting human facial features. Compared with other methods such as multi-scale retinex and self-quotient image, when Yale B was used as the face database for the test, the DRG method yielded 97.8% accuracy, indicating that this method can more effectively eliminate the influences of illumination variations on human facial features and increase face recognition rates.*

**Keywords:** face recognition, relative gradient method, rank transform, dual-tree complex wavelet transform, principal component analysis

---

1. **Introduction.** Face recognition is broadly employed in various fields, such as entry access control, criminal identification, safety identification of financial withdrawal, and user identification for online transactions. Because the extraction of facial image features is non-intrusive, face recognition is a highly suitable identification method. Most face recognition systems are based on core technologies, such as face detection, face location, and facial feature extraction. These core technologies generally require high image quality and a controlled environment. However, such conditions cannot be easily achieved in natural environments. Moreover, the following factors exert a substantial influence on the effectiveness of face recognition: differing viewpoints, illumination variation, and changes in facial expressions. Compared with differing viewpoints and changes in facial expressions, illumination variations typically exert a greater influence on the detection of inherent human facial features. This phenomenon increases the importance of illumination variation processing in face recognition systems.

Face recognition techniques can be divided into two major approaches that involve holistic or local methods. Holistic approaches include principal component analysis (PCA) [1, 2], linear discriminant analysis (LDA) [3, 4], and independent component analysis (ICA) [5, 6], whereas local approaches [7, 8] involve edge gradients [9, 10], the dual-tree complex

wavelet transform (DT-CWT) [11, 12], local binary patterns (LBPs) [13, 14], and the scale-invariant feature transform [15, 16].

Numerous studies have investigated the application of local methods for face recognition, particularly illumination variation processing. First, illumination uniformity processing should be conducted on image illumination variations. Wang et al. [17] and Shashua et al. [18] performed face recognition by transforming images of targeted human faces into those in which factors corresponding to lighting were removed. Belhumeur et al. [19] proposed a 3D face model, which can be used to theoretically re-render 2D images of human faces for all lighting conditions at fixed viewpoints, thereby resolving the problem of illumination variation. Lu et al. [20], Lee et al. [21], and Chen et al. [22] conducted linear transformations of the gray intensity distribution between pixels based on intensity variation differences. This method was used to establish normalized images and reduce the influence that illumination non-uniformity exerts on the images of human facial features. Rahman et al. [23] proposed the multi-scale retinex (MSR) model to achieve a balance between dynamic range compression and tonal rendition and maintain image edges and color information, thereby achieving contrast enhancement. Wang et al. [24] normalized human face images under varying lighting conditions by using technologies such as image morphology and self-quotient images (SQI) according to the human face luminance characteristics. Additionally, they developed this approach into dynamic methods for estimating luminance to eliminate the effects of illumination variations and retain facial features.

Numerous methods for extracting facial features have been proposed [1-16], among which, the DT-CWT provides good directional selectivity and accurate phase space information regarding the high-frequency portions of images. Ya and Lian [25] used the DT-CWT to propose a rotational invariant pattern algorithm based on log-polar mapping and DT-CWT. Xie et al. [26] used DT-CWT to conduct a 5-scale transformation of facial images to extract facial eigenvectors, and subsequently employed a support vector machine for classification. Huang et al. [27] extracted facial features by leveraging the advantages of the DT-CWT method (i.e., the good directional selectivity and shift invariance, as well as its robustness to variations in illumination and facial expressions).

To mitigate the influence of illumination variations on human facial features, an illumination variation processing method is proposed in this study. We used the diagonal relative gradient (RG) method (hereafter referred to as the DRG method) to eliminate the influence that illumination variations have on facial features. In addition, the rank transform method was adopted to enhance images of facial features. Subsequently, we employed the DT-CWT to extract facial features from the enhanced images and the PCA to reduce the dimension of the facial images. Finally, we used the Euclidean distance (ED) for feature classification and produce classification results.

The remainder of this paper is organized as follows: The proposed face recognition method based on the DRG method under varying illumination is introduced in Section 2. Experimental results to demonstrate the performance of the proposed method are presented in Section 3. Finally, concluding remarks are provided in Section 4.

**2. The proposed method.** The proposed face recognition method is shown in Fig. 1. According to this flowchart, the method can be divided into the following procedures: (1) Smooth the input facial images using a Gaussian filter; (2) use the DRG method to eliminate the influence of illumination variations; (3) enhance the facial features in the input images using the rank transform method; (4) apply the DT-CWT to extract facial features [27]; (5) employ PCA to reduce the facial feature dimensions; and (6) adopt ED

to classify the facial features and output classification results. These technologies are specifically explained later in this paper.

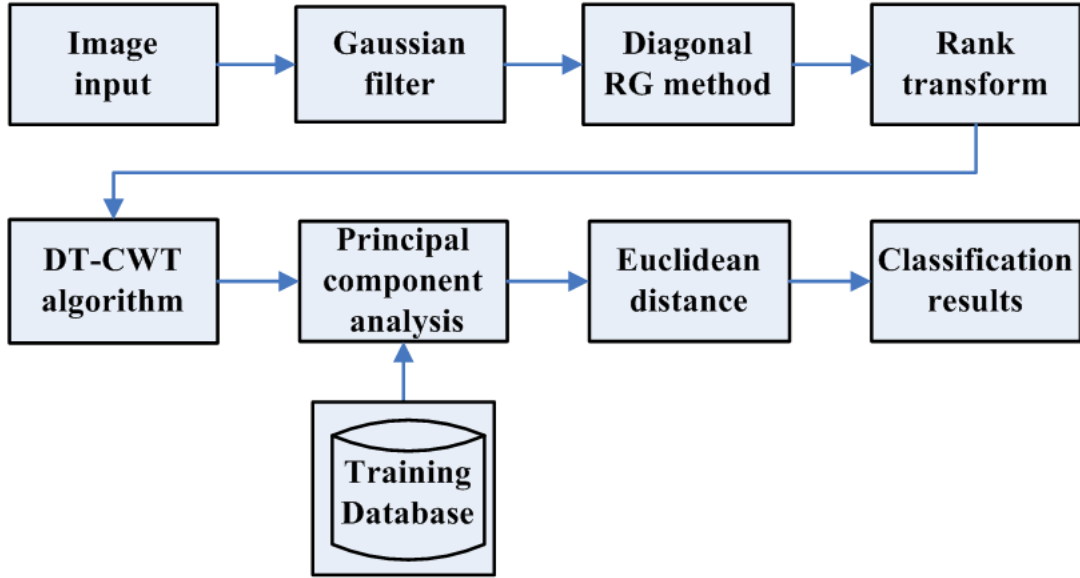


FIGURE 1. Flowchart of the proposed method for face recognition

**2.1. DRG Method.** Under certain lighting conditions, the image grayscale value  $I(x, y)$  is the product of the reflectance component  $R(x, y)$  and illuminance component  $L(x, y)$  on object surfaces, and can be expressed as

$$I(x, y) = R(x, y)L(x, y). \quad (1)$$

The luminance component  $L(x, y)$  is determined by the external lighting sources, and the reflectance component  $R(x, y)$  is dependent on the characteristics of the object surfaces. Based on common assumptions, the illuminance component  $L(x, y)$  of an image varies slowly, whereas the reflectance component  $R(x, y)$  varies rapidly. Thus, the illuminance component  $L(x, y)$  is the low-frequency portion of signals and the reflectance component  $R(x, y)$  is the high-frequency portion of signals [28]. According to the common assumptions, considering that  $(x, y)$  and  $(x + \Delta x, y)$  are two adjacent points in a grayscale image  $I(x, y)$ , because  $L(x, y)$  is determined by only external light sources, when  $\Delta x$  is small, the assumption of  $L(x, y) \approx L(x + \Delta x, y)$  is valid. Similarly, when  $\Delta y$  is small,  $L(x, y) \approx L(x, y + \Delta y)$  can be inferred. The aforementioned analysis indicates that the gradient  $\nabla I(x, y)$  of a grayscale image  $I(x, y)$  can be calculated using the following formula:

$$\nabla I(x, y) = \frac{\partial I(x, y)}{\partial x} + \frac{\partial I(x, y)}{\partial y} \doteq L(x, y) \left\{ \frac{\partial R(x, y)}{\partial x} + \frac{\partial R(x, y)}{\partial y} \right\} \quad (2)$$

We defined the relative gradient of the grayscale image  $I(x, y)$  as  $\nabla_r I(x, y) = \nabla I(x, y) / I(x, y)$ . Thus, Eq. (2) can be rewritten as

$$\begin{aligned} \nabla_r I(x, y) &= \left( \frac{\partial I(x, y)}{\partial x} + \frac{\partial I(x, y)}{\partial y} \right) / I(x, y) \\ &\doteq \left\{ \frac{\partial R(x, y)}{\partial x} + \frac{\partial R(x, y)}{\partial y} \right\} / R(x, y) = \nabla_r R(x, y) \end{aligned} \quad (3)$$

According to Eq. (3), the RG value  $\nabla_r I(x, y)$  of a grayscale image  $I(x, y)$  is approximately equal to the RG value  $\nabla_r R(x, y)$  of the reflectance component  $R(x, y)$ . Furthermore, the gradient angle of a grayscale image  $I(x, y)$  at  $(x, y)$  can be calculated as

$$\theta(x, y) = \tan^{-1}\left(\frac{\partial I(x, y)/\partial y}{\partial I(x, y)/\partial x}\right). \quad (4)$$

Fig. 2 can be used to illustrate the method for calculating the horizontal and vertical gradient values, i.e.,  $\partial I(x, y)/\partial x$  and  $\partial I(x, y)/\partial y$ , of a grayscale image  $I(x, y)$ , which can be expressed in Eq. (5) and Eq. (6), respectively.

$$\frac{\partial I(x, y)}{\partial x} = \frac{I(x+1, y) - I(x-1, y)}{2} \quad (5)$$

$$\frac{\partial I(x, y)}{\partial y} = \frac{I(x, y+1) - I(x, y-1)}{2} \quad (6)$$

The relative gradient  $\nabla_r I(x, y)$  of a grayscale image  $I(x, y)$  can be determined by substituting Eq. (5) and Eq. (6) into Eq. (3) as

$$\nabla_r I(x, y) = \frac{1}{2} \left( \frac{I(x+1, y) - I(x-1, y)}{I(x, y)} + \frac{I(x, y+1) - I(x, y-1)}{I(x, y)} \right). \quad (7)$$

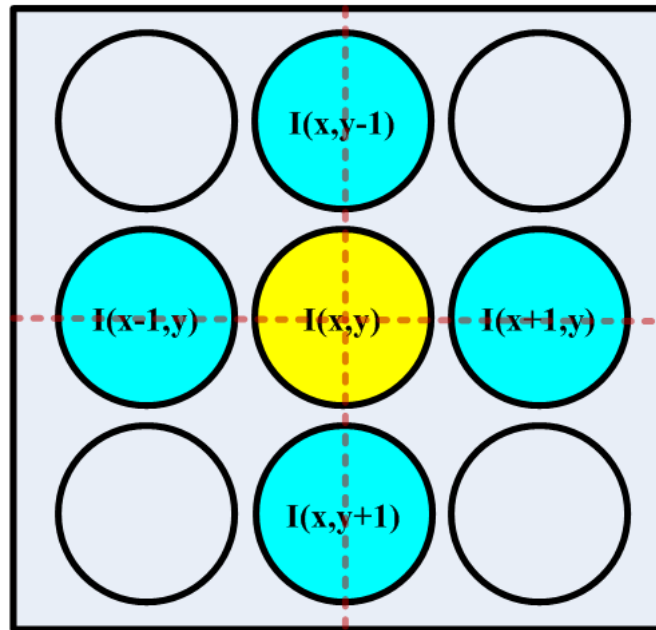


FIGURE 2. Schematics of calculating horizontal and vertical gradients for gray images

Unlike the aforementioned method for calculating the horizontal and vertical RG of grayscale images, we suggested using the DRG method to calculate the edge data of images. This calculation method is illustrated in Fig. 3.

According to Eq. (7), we redefined the DRG  $\nabla_r^d I(x, y)$  of a grayscale image  $I(x, y)$  as.

$$\nabla_r^d I(x, y) = \frac{1}{2\sqrt{2}} \left( \frac{I(x+1, y+1) - I(x-1, y-1)}{I(x, y)} + \frac{I(x-1, y+1) - I(x+1, y-1)}{I(x, y)} \right). \quad (8)$$

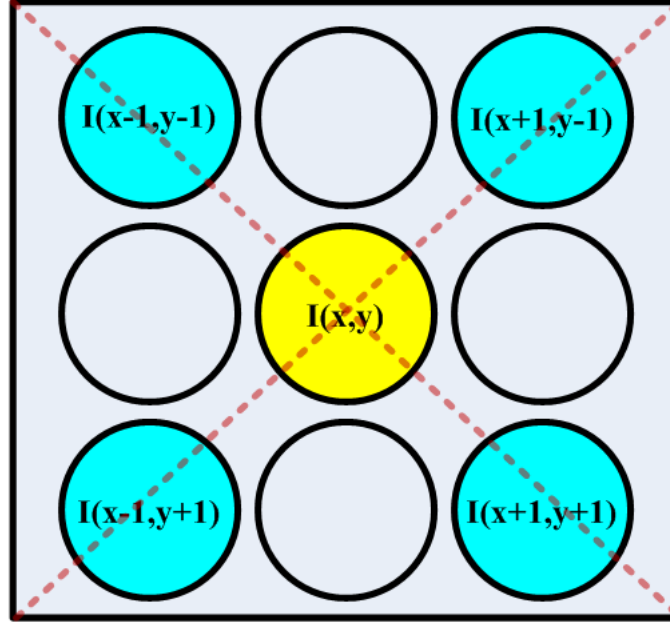


FIGURE 3. Schematics of calculating diagonal gradient for gray images

The denominator in Eq. (8) is  $2\sqrt{2}$ . As shown in Fig. 3, the diagonal length is  $\sqrt{2}$  of the length of the corresponding side. When determining  $\nabla_r^d I(x, y)$  using Eq. (8), to prevent the grayscale value at the center point  $(x, y)$  equaling 0, the RG values were only calculated when the grayscale values at  $(x, y)$  do not equal 0. When the grayscale value at the center point  $(x, y)$  is 0, we let the corresponding RG values equal 0. The experimental results indicated that compared with horizontal and vertical RG methods, the DRG method yields superior images of facial features (see Fig. 4).



FIGURE 4. Facial feature extraction by different RG methods. (a) Original image, (b) horizontal and vertical RG image; (c) DRG image

**2.2. Rank Transform.** Histogram remapping is typically employed as an image preprocessing method, specifically the rank transform method (hereafter referred to as RANK), which increases the uniformity of histogram distributions in transformed images. Let the width and height of grayscale images  $I(x, y)$  be  $W$  and  $H$ , respectively, then the total number of image pixels is  $N (= W \times H)$ . During the process of RANK, we transformed 2D images  $I(x, y) \in \mathfrak{R}^{W \times H}$  into a 1D column vector  $\mathbf{u}(\xi) \in \mathfrak{R}^N$ , where  $0 \leq \xi \leq N - 1$ . Subsequently, The column vector was sorted according to the grayscale values (i.e.,  $\mathbf{u}(\xi)$ ), and the sorting result is denoted as  $\mathbf{v}(\xi)$ . We then specified a rank value  $\Phi$  ( $0 \leq \Phi \leq N - 1$ )

for  $v(\xi)$ , where  $0 \leq \xi \leq N - 1$ . The formula for calculating the rank values is expressed as Eq. (9).

$$\frac{N - \Phi + 0.5}{N} = F(t) = \int_{\varsigma=-\infty}^t f(\varsigma) d\varsigma \quad (9)$$

and

$$f(\varsigma) = \frac{1}{\sigma\sqrt{2\pi}} \exp\left(-\frac{(\varsigma - \mu)^2}{2\sigma^2}\right) \quad (10)$$

where  $f(\varsigma)$  represents the Gaussian normal distribution function, and  $\mu$  and  $\sigma$  represent the mean and standard deviation, respectively.  $F(t)$  represents the cumulative distribution function (CDF), which varies with the integral-valued upper limit  $t$  in Eq. (9). In this paper,  $\mu = 0$  and  $\sigma = 1$  are used. If the CDF  $F(t) = \gamma$ , the mapping value  $t = F^{-1}(\gamma)$  can be obtained, where  $F^{-1}$  represents the inverse function of  $F$ .

As shown in Fig. 5, the dark raw image was transformed into an image of superior quality through RANK. The image in Fig. 5(c) clearly shows the details on the human face. The histogram distribution shown in Fig. 5(d) exhibits a normal gaussian distribution. Comparing Fig. 5(b) with Fig. 5(d), the contrast in Fig. 5(d) is greater than that in Fig. 5(b). In addition, the histogram distribution shown in Fig. 5(d) possesses higher uniformity than that in Fig. 5(b). As demonstrated in Fig. 6, applying RANK to the image processed using the DRG method further enhanced the inherent features of the human face.

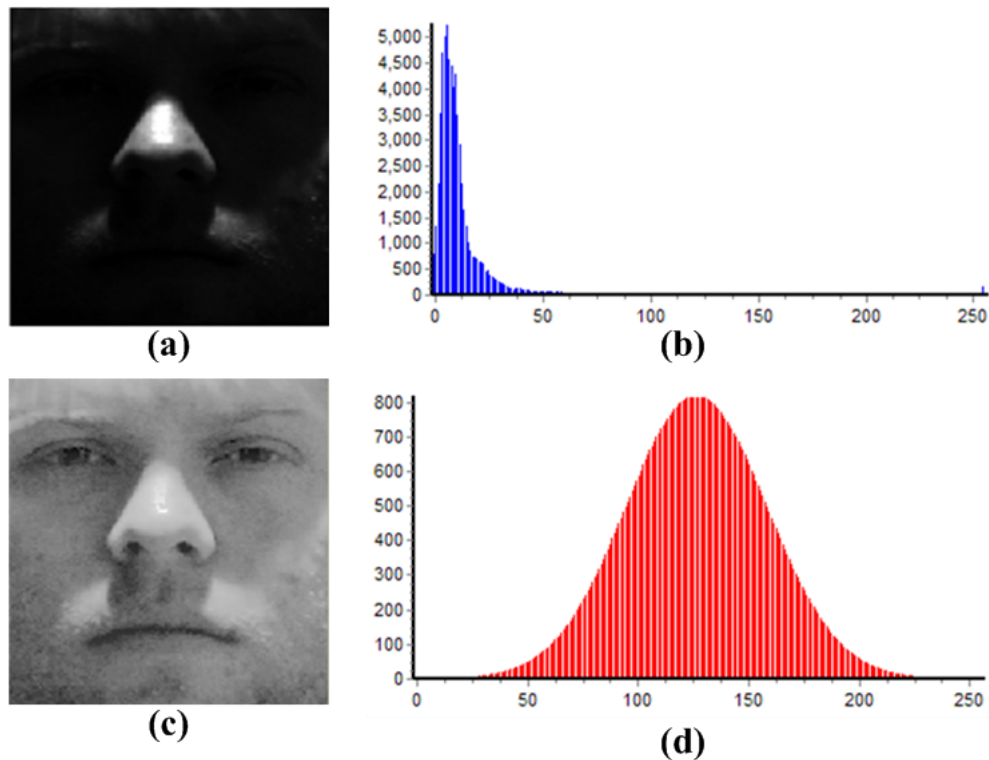


FIGURE 5. Image processing by rank transform. (a) Original image, (b) histogram of (a), (c) image after rank transform, and (d) histogram of (c)

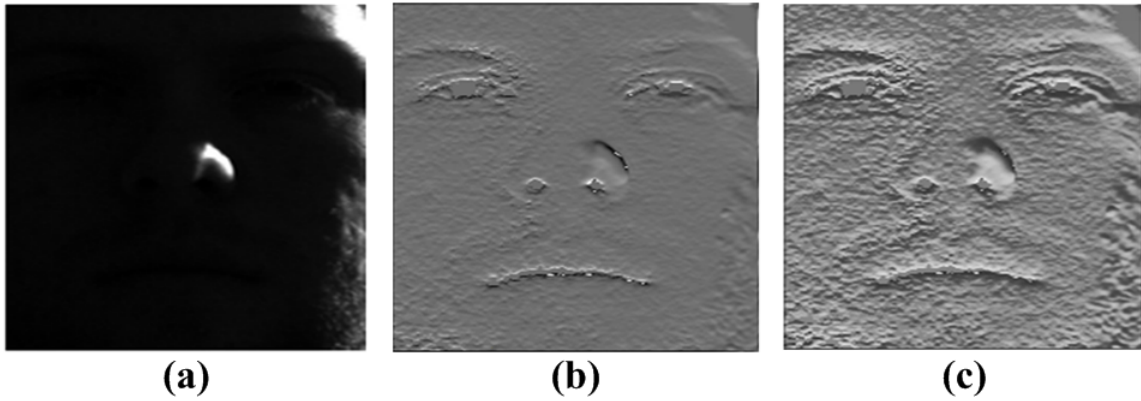


FIGURE 6. (a) Original image, (b) image processing by DRG method, and (c) image processing by rank transform of (b)

**2.3. DT-CWT Facial Feature Extraction.** Compared with the discrete wavelet transform, the DT-CWT (see Fig. 7) proposed by Kingsbury [29] in 1999 yields shift invariance. Additionally, the DT-CWT provides six orientations (i.e.,  $\pm 15^\circ$ ,  $\pm 45^\circ$ , and  $\pm 75^\circ$ ). Thus, the DT-CWT possesses good directional selectivity and accurate phase space information. DT-CWT can be conducted by simultaneously applying two sets of filters to the input image data. The transform can be divided into Trees A and B. Tree A is the real part, where  $h_0(n)$  and  $h_1(n)$  represent a low- and high-pass filter, respectively, and the corresponding real-valued scale function is  $\varphi_h(t)$  and the wavelet function is  $\psi_h(t)$ . Tree B is the imaginary part, where  $g_0(n)$  and  $g_1(n)$  represent a low- and high-pass filter, respectively, and the corresponding imaginary-valued scale function and wavelet function are denoted as  $\varphi_g(t)$  and  $\psi_g(t)$ , respectively.

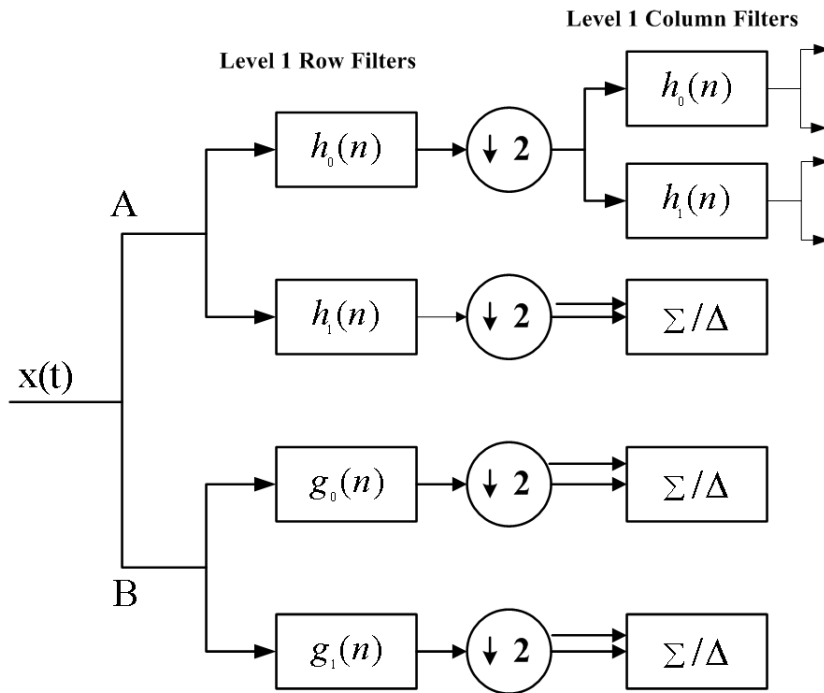


FIGURE 7. Framework of the first stage of DT-CWT

The DT-CWT decomposition process is shown in Fig. 7. Each stage can be further decomposed into two low-frequency bands and six high-frequency bands. The overall redundancy remained 4:1 independent of the number of stages. We can then use the details of the six high-frequency bands in each decomposition stage to produce information on the images for the six directions ( $\pm 15^\circ$ ,  $\pm 45^\circ$ , and  $\pm 75^\circ$ ). The six angles of Tree A transform can be calculated using

$$Re \begin{cases} \psi_i(x, y) = \frac{1}{\sqrt{2}}(\psi_{1,i}(x, y) - \psi_{2,i}(x, y)) \\ \psi_{i+3}(x, y) = \frac{1}{\sqrt{2}}(\psi_{1,i}(x, y) + \psi_{2,i}(x, y)) \end{cases} \quad \text{where } 1 \leq i \leq 3, \quad (11)$$

where the wavelet function of the Tree A transform is represented as

$$\begin{aligned} \psi_{1,1}(x, y) &= \varphi_h(x)\psi_h(y) & \psi_{2,1}(x, y) &= \varphi_g(x)\psi_g(y) \\ \psi_{1,2}(x, y) &= \psi_h(x)\varphi_h(y) & \text{and } \psi_{2,2}(x, y) &= \psi_g(x)\varphi_g(y) . \\ \psi_{1,3}(x, y) &= \psi_h(x)\psi_h(y) & \psi_{2,3}(x, y) &= \psi_g(x)\psi_g(y) \end{aligned} \quad (12)$$

The six angles of the Tree B transform are defined as

$$Im \begin{cases} \psi_i(x, y) = \frac{1}{\sqrt{2}}(\psi_{3,i}(x, y) + \psi_{4,i}(x, y)) \\ \psi_{i+3}(x, y) = \frac{1}{\sqrt{2}}(\psi_{3,i}(x, y) - \psi_{4,i}(x, y)) \end{cases} \quad \text{where } 1 \leq i \leq 3, \quad (13)$$

where the wavelet function of the Tree B transform is represented as

$$\begin{aligned} \psi_{3,1}(x, y) &= \varphi_g(x)\psi_h(y) & \psi_{4,1}(x, y) &= \varphi_h(x)\psi_g(y) \\ \psi_{3,2}(x, y) &= \psi_g(x)\varphi_h(y) & \text{and } \psi_{4,2}(x, y) &= \psi_h(x)\varphi_g(y) . \\ \psi_{3,3}(x, y) &= \psi_g(x)\psi_h(y) & \psi_{4,3}(x, y) &= \psi_h(x)\psi_g(y) \end{aligned} \quad (14)$$

Thus, 12 high-frequency images can be obtained using Eq. (11) and Eq. (13). Fig. 8 shows two rows of frequency spectrum images of the real and imaginary parts in six directions. Generally, when images are processed in the first stage of the DT-CWT, 16 sub-images can be obtained, of which 12 are high-frequency images and 4 are low-frequency images. We employed the method introduced in [27] to extract facial features. In other words, only the four low-frequency images were used. These four images underwent pairwise subtraction to obtain six difference images. All difference images were expressed as 1D column vectors, that is,  $\Delta I^{(i)}(x, y) \in \mathbb{R}^N$ ,  $i = 1, 2, \dots, 6$ , where  $N = W \times H$ . Finally, the six difference images were concatenated, forming facial eigenvectors.

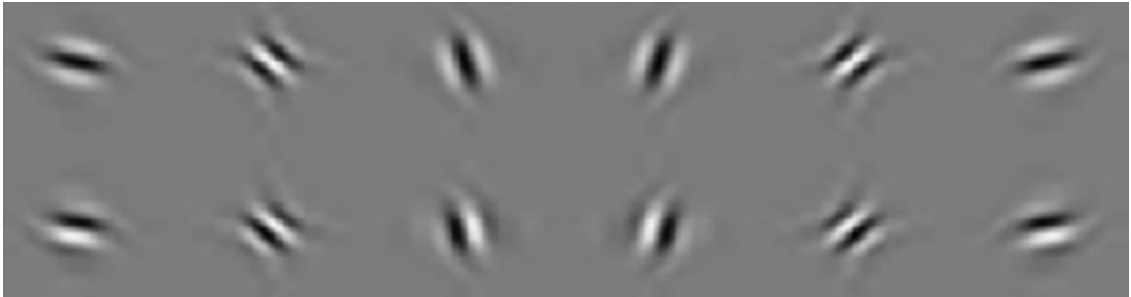


FIGURE 8. Power spectrum of six different angles for real part in upper row and for imaginary part in bottom row

**2.4. PCA Feature Dimension Reduction and Feature Classification.** PCA transformation primarily uses the concept of the least mean square error to achieve optimal correlation and reduce data dimension. Let a grayscale image be  $I_k \in \mathfrak{R}^{W \times H}$ ,  $k = 1, 2, \dots, M$ , and it can be further converted into 1D column vector as  $\Gamma_k \in \mathfrak{R}^N$  ( $N = W \times H$ ). The average facial vector  $\Psi$  of the training set was calculated using

$$\Psi = \frac{1}{M} \sum_{k=1}^M \Gamma_k. \quad (15)$$

Subsequently, the average facial vector  $\Psi$  was subtracted from each facial vector  $\Gamma_k$  to obtain  $\Phi_k = \Gamma_k - \Psi$ . Additionally,  $\Phi_k$  was used to calculate the covariance matrix according to the following formula:

$$C_{N \times N} = \frac{1}{M} \sum_{k=1}^M \Phi_k \Phi_k^T \quad (16)$$

The eigenvector of covariance matrix  $C_{N \times N}$  was  $\mathbf{u}_k$ ,  $k = 1, 2, \dots, N$ , which is an orthonormal vector. The first  $K$  eigenvectors that corresponded to large eigenvalues were used to approximate the test image  $\Phi_k$ . The obtained approximate image  $\hat{\Phi}_k$  spanned by eigenvectors  $\mathbf{u}_k$  can be expressed as

$$\hat{\Phi}_k = \Psi + \sum_{k=1}^K w_k \mathbf{u}_k \quad (w_k = \mathbf{u}_k^T \Phi_k), \quad (17)$$

where  $\mathbf{u}$  represents the facial eigenvector, and  $\mathbf{w} \in \mathfrak{R}^K$  represents the vector of projection coefficients of the test images in the eigenspace. Finally, Euclidean distance classifiers were used to compare the projection coefficients of the test images ( $\mathbf{w}^{TEST}$ ) and training sample ( $\mathbf{w}^{TRAIN}$ ) for feature classification. The corresponding formula is shown below.

$$dist(\mathbf{w}^{TEST}, \mathbf{w}^{TRAIN}) = \sqrt{\sum_{k=1}^K (\mathbf{w}_k^{TEST} - \mathbf{w}_k^{TRAIN})^2} \quad (18)$$

**3. Experimental Results.** The Yale face database B (hereafter referred to as Yale B) and extended Yale face database B (hereafter referred to as Extended Yale B) were adopted for this study [30]. Yale B contained 10 subjects and Extended Yale B contained 28 subjects. In both databases, each facial image featured five angles of lighting directions, generating 64 face images with varying luminance. Because this study was focused on reducing the influence of illumination variations on face recognitions, only frontal images (totally, 2,432 ( $= 38 \times 64$ ) facial images) were employed. All facial images were manually cropped, rendering eyes in all the facial images to be located on the same horizontal level. In addition, the facial images were resized to  $128 \times 128$  pixels (see Fig. 9).

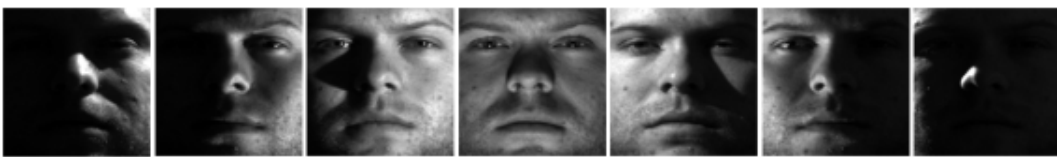


FIGURE 9. Sample images in Yale B and Extended Yale B face database

Yale B can be divided into five subsets according to the angles ( $\theta$ ) between the light source and camera. The angles for Subsets 1 to 5 are  $0^\circ \leq \theta \leq 12^\circ$ ,  $13^\circ \leq \theta \leq 25^\circ$ ,  $26^\circ \leq \theta \leq 50^\circ$ ,  $51^\circ \leq \theta \leq 77^\circ$ , and  $\theta \geq 78^\circ$ , respectively. Subsets 1 to 5 contain 7, 12, 12, 14, and 19 subject images, respectively. Because each subset consists of 10 subjects, Subsets 1 to 5 yield 70, 120, 120, 140, and 190 images. Thus, a total number of 640 facial images are obtained from the 5 subsets. The typical samples for subsets 1 to 5 in Yale B are shown in Fig. 10.



FIGURE 10. Sample images in Subset 1 to Subset 5 in Yale B face database

To verify that the DRG method is superior to the traditional RG method for facial feature extraction, this study employed the Yale B database for the experiment. The experiment selected one image (the images marked with a red border) in turn from Fig. 10 as the training sample. The remaining facial images were used as test samples. Therefore, each of the 10 subjects in the Yale B database possessed one training image and 63 test images. In other words, 10 training images and 630 test images were employed for each experiment. The face recognition rates are presented in Fig. 11. Based on this data, the DRG method combined with RANK (DRG+RANK) yielded higher face recognition rates

compared with that of the traditional RG method combined with RANK (RG+RANK). This indicates that DRG+RANK offers higher facial feature extraction abilities than those of RG+RANK. The data shown in Fig. 11 also demonstrates that illumination variations exerted a substantial influence on face recognition rates.

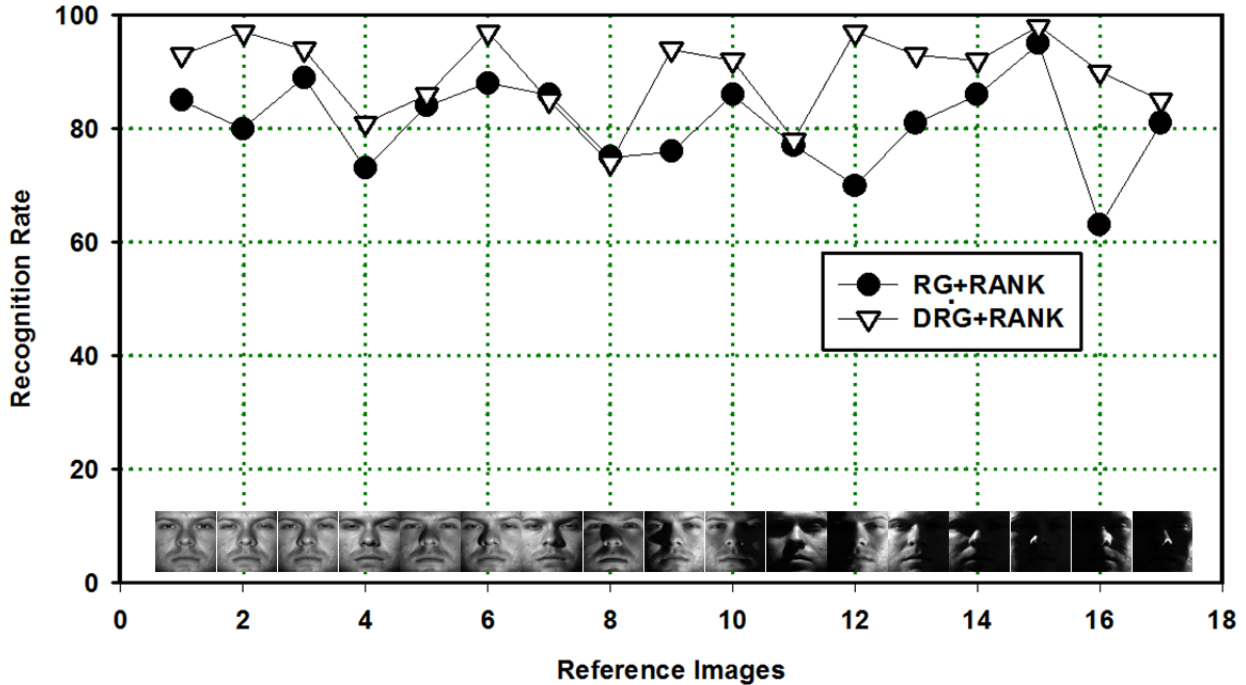


FIGURE 11. Comparison of recognition rate between DRG+RANK and RG+RANK methods using Yale B face database

This study aimed to verify that the proposed DRG+RANK method yields higher illumination variation resistance (i.e., higher face recognition rates) compared with relevant methods proposed in previous studies [23, 24] and traditional RG methods. For Experiment 1, Subset 1 of Yale B was adopted as the training samples because Subset 1 possessed the smallest variations of lighting angle, indicating that they had more uniform luminance (see Fig. 10). Subsets 2 to 5 were employed as the test samples. The experiment results are presented in Table 1 and show that the proposed method yielded the highest face recognition rates for all the subsets when comparing with the MSR [23], SQI [24], and RG methods. Note that the results of MSR and SQI methods are obtained under the same experimental conditions. For Experiment 2, one image per subject, in turn, was selected from Subset 1 to serve as the training set. The remaining images from subsets 1 to 5 were used as the testing sets. Table 2 shows that the recognition rates of different methods on different testing sets. Note that seven experiments were conducted for subsets 1 to 5 because every time we only chose one image per subject from Subset 1 as a training set, in which Subset 1 has seven images for each subject (see Fig. 10). Therefore, the results listed in Table 2 are the average values of the recognition rates of these seven experiments. As shown in Table 2, the proposed method yielded the best results for each subset, with an average recognition rate of 94.7%. The experiment data of MSR and SQI provided in Tables 1 and 2 were referenced from [23] and [24], respectively.

In addition to comparing with MSR [23] and SQI [24], we also compared the DRG method with that introduced in [21]. Lee et al. [21] proposed two methods for reducing illumination variations: Method 1 involves the column-wise linear transformation and

TABLE 1. Performance comparison on Yale B face database for different methods in experiment 1

Method	Subset 2	Subset 3	Subset 4	Subset 5	Average
MSR [23]	<b>100%</b>	91.7%	65.0%	77.4%	83.5%
SQI [24]	99.2%	96.7%	80.7%	84.7%	90.3%
RG_Rank	<b>100%</b>	96.0%	81.0%	86.0%	90.8%
DRG_Rank	<b>100%</b>	<b>100%</b>	<b>93.0%</b>	<b>98.0%</b>	<b>97.8%</b>

Note: The values presented in boldface type are the highest face recognition rates in the subset.

TABLE 2. Performance comparison on Yale B face database for different methods in experiment 2

Method	MSR [23]	SQI [24]	RG_Rank	<b>DRG_Rank</b>
Subset 1	97.1%	96.4%	<b>100%</b>	<b>100%</b>
Subset 2	91.0%	88.1%	96.1%	<b>98.6%</b>
Subset 3	78.8%	85.0%	91.0%	<b>94.0%</b>
Subset 4	62.9%	69.1%	74.3%	<b>88.6%</b>
Subset 5	70.3%	76.6%	73.3%	<b>92.4%</b>
Avg	76.8%	80.6%	86.9%	<b>94.7%</b>

Note: The values presented in boldface type are the highest face recognition rates in the subset.

Method 2 encompasses piece-wise linear transformation of pixel intensity distribution, which corrects and calibrates the grayscale pixel values. In [21], the contents of Yale B and Extended Yale B were adopted as test images. Therefore, 38 subjects were involved in those investigations. For this study, we used Subset 1 as the training sample and Subsets 2 to 5 as test samples to conduct face recognition. The results are presented in Table 3. Method 2 (as proposed by Lee et al. [21]) +LBP yielded the highest face recognition performance, with an average recognition rate of 91.6%. However, the average face recognition rate achieved in this study was 91.7%, which indicates that the proposed method offers superior face recognition and feature extraction abilities. Excluding the data presented for the DRG+RANK method, the data provided in Table 3 was obtained from [21], where HE represents histogram equalization, LN represents local normalization, and LBP represents local binary pattern.

**4. Conclusion.** This study proposed a new DRG method combined with RANK to address the influence of illumination variations on facial images. The results indicated that when Yale B was adopted as the test image samples, and any face image of Subset 1 was selected as the training sample, with the remaining face images used as test samples, the DRG+RANK method yielded superior facial feature extraction abilities than those of traditional RG+RANK. When compared with MSR and SQI, our method could yield an average recognition rate of 94.7%, which exceeds that provided by MSR (76.8%) and SQI (80.6%).

When employing Yale B for the experiment, Subset 1 was used as the training set, and the remaining subsets (i.e., Subsets 2 to 5) were used as the test sets. Our method yielded a face recognition rate of 97.8%, exceeding the rates of 83.5% and 90.3% rendered by MSR

TABLE 3. Performance comparison on Yale B and Extended Yale B face database for different methods

Method	Recognition Rate (%)				
	Subset 2	Subset 3	Subset 4	Subset 5	Average
HE	98.0	80.0	16.0	24.0	54.5
HE + LN	<b>100</b>	98.0	68.0	77.0	85.8
Method 1	<b>100</b>	98.0	66.0	54.0	79.5
Method 2	<b>100</b>	<b>100</b>	83.0	82.0	91.3
LBP	99.6	99.8	83.0	47.0	82.4
HE + LBP	99.6	99.8	83.0	41.0	80.9
Method 1 + LBP	99.6	99.8	<b>89.0</b>	45.0	83.4
Method 2 + LBP	99.6	99.8	89.0	57.0	91.6
DRG + Rank	<b>100</b>	99.8	83.0	<b>84.0</b>	<b>91.7</b>

Note: The values presented in boldface types are the highest face recognition rates in the subset.

and SQI, respectively. When the light source angle range was  $13^\circ \leq \theta \leq 50^\circ$  (Subsets 2 and 3), the proposed method yielded a recognition rate of 100%. In addition, when using Yale B combined with Extended Yale B, the proposed method achieved a recognition rate of 91.7%, exceeding that provided by other effective methods (e.g., 91.6%). Based on the results of comparing DRG+RANK to other methods, DRG+RANK yielded higher facial feature extraction abilities compared with the traditional RG method. Thus, DRG+RANK can more effectively eliminate the influences of illumination variations on facial features to thereby enhance face recognition rates.

**Acknowledgment.** This work was financially supported by the National Science Council, Taiwan, under grant numbers NSC 101-2221-E-212-020 and NSC 102-2221-E-212-015.

## REFERENCES

- [1] A. M. Martinez, and A. C. Kak, PCA versus LDA, *IEEE Trans. Pattern Analysis and Machine Intelligence*, vol. 23, no. 2, pp. 228-233, 2001.
- [2] X. Xie, and K. Lam, Gabor-based kernel PCA with doubly nonlinear mapping for face recognition with a single face image, *IEEE Trans. Image Processing*, vol. 15, no. 9, pp. 2481-2492, 2006.
- [3] G. Dai, and Y. Qian, A gabor direct fractional-step LDA algorithm for face recognition, *Proc. of IEEE International Conference on Multimedia and Expo*, pp. 61-64, 2004.
- [4] D. Jelsovka, R. Hudec, and M. Breznan, Efficient face recognition method based on DCT and LDA, *Proc. of the 34th International Conference on Telecommunications and Signal Processing*, pp. 570-574, 2011.
- [5] J. Yang, D. Zhang, and J. Y. Yang, Constructing PCA baseline algorithms to reevaluate ICA-based face-recognition performance, *IEEE Trans. Systems, Man, and Cybernetics, Part B: Cybernetics*, vol. 37, no. 4, pp. 1015-1021, 2007.
- [6] C. Liu, and H. Wechsler, Independent component analysis of Gabor features for face recognition, *IEEE Trans. Neural Networks*, vol. 14, no. 4, pp. 919-928, 2003.
- [7] C. Schüldt, I. Laptev, and B. Caputo, Recognizing human actions: a local SVM approach, *Proc. of the 17th International Conference on Pattern Recognition*, pp. 32-36, 2004.
- [8] S. Srisuk, and A. Petchpon, Local and holistic texture analysis approach for face recognition, *Proc. of the 17th IEEE International Conference on Image Processing*, pp. 3825-3828, 2010.
- [9] H. S. Xie, and L. G. Wang, Integration classification method of face images based on DT-CWT and SVM, *Journal of Yunnan University Nationalities*, vol. 19, no. 5, pp. 313-316, 2010.
- [10] I. W. Selesnick, R. G. Baraniuk, and N. G. Kingsbury, The dual-tree complex wavelet transform, *Journal of IEEE Signal Processing Magazine*, vol. 22, no. 6, pp. 123-151, 2005.
- [11] H. Tang, Y. Sun, B. Yin, and Y. Ge, Face recognition based on haar LBP histogram, *Proc. of the 3rd International Conference on Advanced Computer Theory and Engineering*, pp. 235-238, 2010.

- [12] H. Zhao, F. Gao, and C. Zhang, A method for face gender recognition based on blocking-LBP and SVM, *Proc. of the 2nd International Conference on Consumer Electronics, Communications and Networks*, pp. 1527-1530, 2010.
- [13] J. Wang, K. N. Plataniotis, and A. N. Venetsanopoulos, Selecting discriminate eigenfaces for face recognition, *Journal of Pattern Recognition Letters*, vol. 26, no. 10, pp. 1470-1482, 2005.
- [14] D. L. Swets, and J. J. Weng, Using discriminant eigenfeatures for image retrieval, *IEEE Trans. Pattern Analysis and Machine Intelligence*, vol. 18, no. 8, pp. 831-836, 1996.
- [15] T. Okakura, and K. Arakawa, Face authentication across age progression using shifted block matching, *Proc. of International Symposium on Intelligent Signal Processing and Communication Systems*, pp. 1-6, 2011.
- [16] N. Kingsbury, Shift invariant properties of the dual-tree complex wavelet transform, *Proc. of IEEE International Conference on Acoustics, Speech and Signal Processing*, pp. 1221-1224, 1999.
- [17] H. T. Wang, S.Z. Li, and Y. S. Wang, Face recognition under varying lighting conditions using self quotient image, *Proc. of the 6th IEEE International Conference on Automatic Face and Gesture Recognition*, pp. 819-824, 2004.
- [18] A. Shashua, and T. Riklin-Raviv, The quotient image: class based re-rendering and recognition with varying illuminations, *IEEE Trans. Pattern Analysis and Machine Intelligence*, vol. 23, no. 2, pp. 129-139, 2001.
- [19] P. N. Belhumeur, and D. J. Kriegman, What is the set of images of an object under all possible lighting conditions?, *International Journal of Computer Vision*, vol. 28, no. 3, pp. 245-260, 1998.
- [20] Y. M. Lu, B. Y. Liao, and J. S. Pan, A Face recognition algorithm decreasing the effect of illumination, *Proc. of International Conference on Intelligent Information Hiding and Multimedia Signal*, pp. 378-381, 2008.
- [21] M. Lee, and C. H. Park, An efficient image normalization method for face recognition under varying illuminations, *Proc. of the 1st ACM international conference on Multimedia information retrieval*, pp. 128-133, 2008.
- [22] C. P. Chen, and C. S. Chen, Lighting normalization with generic intrinsic illumination subspace for face recognition, *Proc. of 10th IEEE International Conference on Computer Vision*, pp. 1089-1096, 2005.
- [23] Z. Rahman, D. Jobson, and G. A. Woodell, Retinex processing for automatic image enhancement, *Journal of Electronic Imaging*, vol. 13, no. 1, pp. 100-110, 2004.
- [24] H. Wang, S. Z. Li, and Y. Wang, Face recognition under varying lighting conditions using self quotient image, *Proc. of the 6th IEEE International Conference on Automatic Face and Gesture Recognition*, pp.819-824, 2004.
- [25] S. Yan, and Q. S. Lian, Rotation invariant texture classification algorithm based on Log-Polar and DT-CWT, *Computer Engineering and Applications*, vol. 43, no. 11, pp. 48-50, 2007.
- [26] H. S. Xie, and L. G. Wang, Integration classification method of face images based on DT-CWT and SVM, *Journal of Yunnan University Nationalities*, vol. 19, no. 5, pp. 313-316, 2010.
- [27] D. Y. Huang, S. H. Dai, T. W. Lin, and W. C. Hu, Face Recognition based on dual-tree complex wavelet transform wavelet transform, *Proc. of National Computer Symposium*, 2013.
- [28] H. Hu, Multiscale illumination normalization for face recognition using dual-tree complex wavelet transform in logarithm domain, *Computer Vision and Image Understanding*, vol. 115, no. 10, pp. 1384-1394, 2011.
- [29] N. G. Kingsbury, Complex wavelets for shift invariant analysis and filtering of signals, *Applied and computational harmonic analysis*, vol. 10, no. 3, pp. 234-253, 2001.
- [30] Center for Computational Vision and Control, Yale B Face Database, <http://cvc.yale.edu/projects/yalefacesB/yalefacesB.html>.